Characterization of hydrogen-like states in bulk $Si_{1-x}Ge_x$ alloys through muonium observations

2005 J. Phys.: Condens. Matter 17 4567

(http://iopscience.iop.org/0953-8984/17/28/015)

INSTITUTE OF PHYSICS PUBLISHING JOURNAL OF PHYSICS: CONDENSED MATTER

J. Phys.: Condens. Matter **17** (2005) 4567–4578 doi:10.1088/0953-8984/17/28/015

Characterization of hydrogen-like states in bulk $Si_{1-x}Ge_x$ alloys through muonium observations

P J C King[1], R L Lichti[2], S P Cottrell[1], I Yonenaga[3] and B Hitti[4]

[1] ISIS Facility, Rutherford Appleton Laboratory, Chilton, Oxfordshire OX11 0QX, UK
[2] Physics Department, Texas Tech University, Lubbock, TX 79409-1051, USA
[3] Institute for Materials Research, Tohoku University, Japan
[4] TRIUMF, 4004 Wesbrook Mall, Vancouver, BC, V6T 2A3, Canada

E-mail: philip.king@rl.ac.uk

Received 6 April 2005
Published 1 July 2005
Online at stacks.iop.org/JPhysCM/17/4567

Abstract

Much of our knowledge of the charge states, lattice site and behaviour of hydrogen in bulk semiconductors comes from observation of its muonium analogue. Here we present studies of muonium behaviour across the composition range in bulk, Czochralski-grown $Si_{1-x}Ge_x$ alloy material, focusing in particular on the muonium hyperfine parameters. For the bond-centred muonium species, a broad distribution of parameters is observed, consistent with a variety of bonding environments. The average value of the isotropic component of the bond-centred hyperfine parameter shows a linear variation with alloy composition, which might be expected based on the linear variation with composition of alloy bond lengths. In contrast, the hyperfine parameter of the tetrahedral-site muonium species (Mu_T) appears to vary non-linearly with alloy composition, and an explanation of this in terms of Mu_T mobility is provided. The temperature dependence of the Mu_T hyperfine parameter observed in several alloy compositions is compared with that seen in pure Si. Previous descriptions of the low-temperature behaviour of the Mu_T parameter in Si are discussed in the light of results from $Si_{1-x}Ge_x$ material.

(Some figures in this article are in colour only in the electronic version)

1. Introduction

Hydrogen is a common impurity in semiconducting materials, particularly in material produced from hydrogen-containing precursors. In general acting as an amphoteric dopant and removing electronic levels from the bandgap, its effects can be beneficial, for example in the passivation of dangling bonds in amorphous silicon, or deleterious in the case of passivation of desirable dopants. Very significant experimental and computational effort is expended

in trying to understand and predict its behaviour, and the recent discovery of its ability to act as a shallow dopant to enhance conductivity in some materials has generated much interest [1].

Direct study of the behaviour of isolated hydrogen in semiconductors can in many cases be very difficult or impossible, partly because of the high reactivity of hydrogen impurities. One way of gaining insight into proton and hydrogen activity is by studying the muon or muonium analogue [2]. Muons have a mass of roughly one-ninth that of the proton, and so the positive muon can be thought of as a light proton isotope. The light hydrogen-like atom *muonium*, formed when a positive muon picks up an electron, is electronically almost identical to isolated hydrogen, and so provides a good guide to hydrogen electronic states [3]. Much of our understanding of hydrogen behaviour in semiconducting materials—sites, electronic levels, etc—has come through muonium observations. For example, in silicon and germanium two muonium states are formed at low temperatures: an immobile, bond-centred species Mu_{BC}, and a rapidly-diffusing tetrahedral-site centre Mu_T. Detailed models have been built up describing their behaviour and interactions [4, 5]. More recent examples include the discovery of shallow donor hydrogen states in III–V and II–VI materials through muon investigations [6, 7], with examples of later confirmation by other techniques [8].

1.1. Studies of bulk $Si_{1-x}Ge_x$ alloy properties

In this paper we focus on muonium studies in bulk $Si_{1-x}Ge_x$ alloys. $Si_{1-x}Ge_x$ material has generated much attention due to its ability to provide new electronic functionality whilst using existing silicon-device fabrication technology. Applications have typically focused on strained-layer $Si_{1-x}Ge_x$ material, grown epitaxially on to Si or $Si_{1-y}Ge_y$ substrates, where interest lies in transistor manufacture and the possibility of including optoelectronic components within Si-based integrated circuits [9]. Uses of epitaxial $Si_{1-x}Ge_x$ layers have generated interest in the bulk, unstrained $Si_{1-x}Ge_x$ material, and Czochralski growth of alloy material is possible (for example [10]). This has enabled investigation of the intrinsic properties of the bulk alloy, including dislocation behaviour [11], thermal and electronic properties [12], photoconductivity [13], alloy crystal structure [14], properties of doped material [15, 16] and phonon behaviour [17]. In addition, bulk alloy material offers potential applications in the manufacture of radiation detectors due to its greater stability against radiation damage and improved sensitivity compared with silicon [18, 19].

With regard to impurity behaviour in bulk $Si_{1-x}Ge_x$ material, studies are limited, particularly ones which span the alloy composition range. The lattice location of dissolved oxygen has been investigated [20], and studies of the oxygen–vacancy complex [21] and carbon-related defects [22] have been made in low-Ge material. In the case of hydrogen, DLTS investigations [23], infrared absorption [24] and theoretical work [25] have focused on the bond-centred hydrogen species in low-Ge material, with some modification of the vibrational modes and electrical levels of this species being seen compared with pure Si due to altered bonding environments. In Ge with very dilute Si impurities there is evidence for the electrical activation of impurity atoms by H [26]. Strong interaction between the tetrahedral muonium species and Si impurities in Ge has also been observed [27].

More recently, the availability of bulk $Si_{1-x}Ge_x$ alloy material has enabled more detailed studies of muonium behaviour over a wide range of alloy compositions [28–30]. The aim of the present paper is to extend this work and, in particular, to focus on measurements of the hyperfine parameters of the bond-centred and tetrahedral muonium species, initial presentation of which has been given in [29, 30].

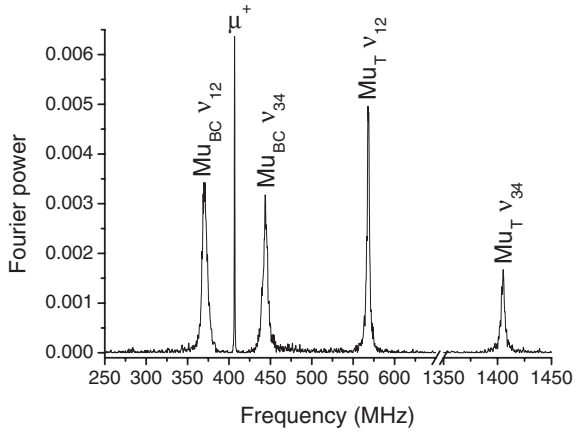

Figure 1. Fourier spectrum of high-transverse-field data (applied field of 3 T) taken from alloy with $x = 0.20$ at 55 K. Diamagnetic muon, Mu_{BC} and Mu_T lines are indicated.

2. Experimental details

2.1. $Si_{1-x}Ge_x$ alloy material

$Si_{1-x}Ge_x$ alloys were grown by the Czochralski method at the University of Tohoku [10]. Single-crystal samples with $x = 0.09$, 0.2, 0.45, 0.6 and 0.77 have been used for this study, in the form of [100] single-crystal wafers ∼0.5 mm in thickness and varying in diameter from over 20 mm for samples with low x to 5–7 mm for intermediate alloy compositions. Alloy compositions were determined by energy-dispersive x-ray analysis. A single alloy sample with $x = 0.11$ was also available from Virginia Semiconductor in the form of a [100] wafer 330 μm in thickness, with a resistivity of 22 Ω cm, also grown by the Czochralski method.

2.2. The muon technique

The muon method [31] involves implantation of spin-polarized, positive muons, and observation of the muon polarization behaviour inside the sample through detection of the positrons emitted when the muons decay (mean muon lifetime $\tau_\mu = 2.2$ μs). Muon measurements were performed at the TRIUMF continuous muon facility in Canada and at the ISIS pulsed muon facility at the Rutherford Appleton Laboratory in England. As a continuous facility, TRIUMF is particularly suited to measurement of high muon precession frequencies (produced using magnetic fields of several tesla applied transverse to the initial muon polarization direction) which cannot be made at a pulsed facility. ISIS, on the other hand, is ideal for measurements requiring application of a pulsed stimulation such as RF-radiation, which can be synchronized to the muon pulse arrival. Measurements in applied fields parallel to the initial muon polarization direction (longitudinal fields) were also made at ISIS.

Measurements at TRIUMF were performed in a transverse field of 3 T using the Belle and HighTime spectrometers on the M15 beamline. These spectrometers are optimized for high-frequency measurements, with the four scintillation counters for positron detection in close proximity to the sample and with sample and scintillators being mounted inside a horizontal flow-cryostat to provide variable temperatures (from room temperature to around 5 K). Figure 1 shows a typical high transverse field Fourier spectrum, taken in 3 T from a $Si_{0.80}Ge_{0.20}$ sample at 55 K. Five clear lines are visible, corresponding either to diamagnetic muons precessing at their Larmor frequency (line at 407 MHz, assumed to be μ^+), or to transitions between the energy levels of paramagnetic muonium species (the Mu_{BC} ν_{12} and ν_{34} lines can be seen at

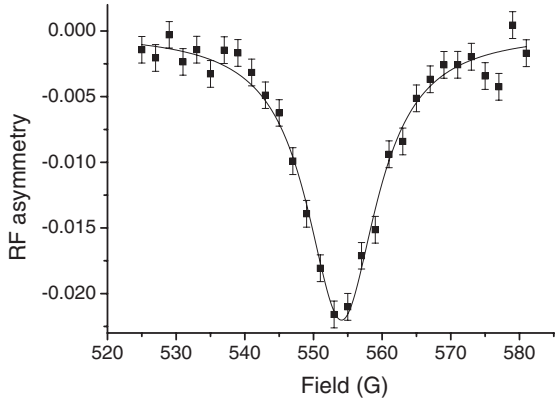

Figure 2. Radio-frequency μSR resonance curve of the Mu_T ν_{12} transition at 500 MHz taken from the $x = 0.09$ sample at 55 K, together with a Lorentzian fit.

370 and 440 MHz respectively, and the Mu_T ν_{12} and ν_{34} lines are visible 570 and 1405 MHz respectively).

At ISIS, the EMU spectrometer was used for longitudinal field and low-transverse-field μSR measurements, together with radio-frequency μSR (RF-μSR) studies. Samples were mounted on a cold-finger closed-cycle refrigerator or within an exchange gas flow-cryostat, both providing temperatures down to around 5 K. To minimize counts from muons stopped in material surrounding samples, the 'fly-past' technique [32] was employed. In this case a backing plate the same size as or smaller than the sample was used to suspend the sample in the beam. Muons not hitting the sample were allowed to travel past it into an evacuated tube, removing them from the measurement.

For RF-μSR measurements, samples were wrapped in insulating Kapton tape and wound with typically three turns of thin, copper conducting tape to provide an RF coil. Tests were carried out to ensure that the muons passed through the copper and Kapton tapes and into the sample. The RF-μSR technique [33, 34] involves application of RF radiation to provide an oscillating field transverse to the initial muon polarization direction. At the same time, a static field is applied parallel to the initial polarization direction. Adjusting the static field strength and/or RF frequency to meet a resonance condition for the system causes the muons' spin to experience a torque due to the RF field and to precess about that field. For the present system, the aim was to measure the Mu_T hyperfine parameter. To do this, a suitable line in the muonium energy level diagram was selected and the resonance position for this line measured. Calculation of muonium energy levels then enabled the hyperfine parameter to be determined from the resonance position. The two most suitable Mu_T resonance lines for such measurements are the ν_{12} and ν_{23} lines, as these have frequencies within the RF measurement range (below $\sim$500 MHz). At low fields ($<$100 G) these lines lie very close to each other, so that it was desirable for the static applied field to be sufficient to separate them; the sensitivity of the position of the lines to changes in hyperfine parameter also increases with applied field. The ν_{12} line was chosen for measurement as it becomes stronger with increasing applied field, whereas the ν_{23} line becomes weaker. The RF frequency was set to 500 MHz at a power level of 100 W, and the static applied field swept to locate the resonance position for the Mu_T ν_{12} line, typically found at around 550 G. Figure 2 shows an RF time-integral resonance curve, taken from the $Si_{0.91}Ge_{0.09}$ sample at 55 K, together with its Lorentzian fit.

It is worthwhile briefly considering the merits of the three different muon techniques which were available for this study: transverse field μSR, RF-μSR and longitudinal field μSR. Transverse field μSR is able to provide accurate measurement of hyperfine parameters by direct observation of muonium precession lines. However, muonium species can only be observed

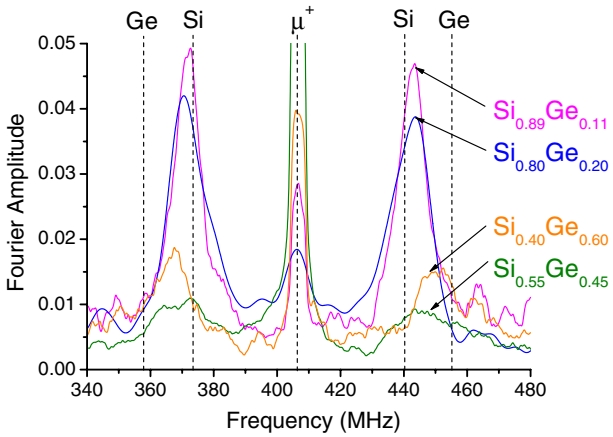

Figure 3. High-transverse-field Fourier spectra from four different alloy compositions in the frequency region of the Mu_{BC} lines. The positions where the line centres would be expected to occur for pure Si and Ge are shown.

by this method when they are formed rapidly compared with the period of the precession signal—any delayed formation leads to a loss of precession phase coherence—and the species must live long enough and have a slow enough relaxation rate for a precession signal to be seen. Longitudinal field μSR and RF-μSR do not have the requirement that the muonium species should be formed promptly, and are sensitive to states produced as the result of conversion of another species. Longitudinal field μSR can be used to identify a muonium species by the field-dependence of the muon polarization—the decoupling of the muon–electron interaction as a function of applied field leads to a characteristic curve from which the hyperfine parameter can be deduced [3]. This technique is sensitive to muonium species which may form very promptly but which also relax rapidly due to, for example, interaction with impurities, but provides the least accurate method of hyperfine parameter measurement.

It is therefore possible that a muonium species observed by one of these techniques may not be seen by another; and such observations can be used to determine whether a species is promptly formed or the result of a conversion process. In the present case, hyperfine parameter measurements have been made using transverse field and RF-μSR, which provide for the most accurate hyperfine parameter values. Longitudinal field μSR was used to deduce the presence of a muonium species when signals from the other techniques were weak.

3. Results

3.1. Bond-centred muonium (Mu_{BC}) hyperfine parameter

Mu_{BC} signals were visible in all the alloy compositions studied. Figure 3 shows the Mu_{BC} ν_{12} and ν_{34} lines produced in high transverse field (3 T, TRIUMF measurements) for four alloy compositions, all taken at around 70 K (the $Si_{0.40}Ge_{0.60}$ data were taken at 50 K). The separation of these two Mu_{BC} lines is given by $A = A_{iso} + (D/2)(3\cos^2\theta - 1)$, A_{iso} and D being the isotropic and dipolar parts of the Mu_{BC} hyperfine parameter and θ being the angle between the Mu_{BC} symmetry axis, a [111] direction, and the applied field. For fields along a [100] crystal direction, as for all samples studied here, $A = A_{iso}$ and the separation of the two lines is a direct measure of the isotropic component of the Mu_{BC} hyperfine parameter.

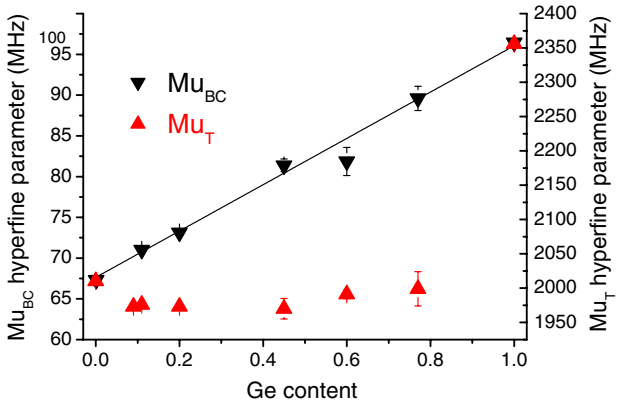

Figure 4. Variation with alloy composition of the average value of the isotropic component of the Mu_{BC} hyperfine parameter, with straight line fit, together with the Mu_T hyperfine parameter (Mu_T values are for 50 K except $x = 0.45$ and 0.77, which are 70 and 75 K respectively).

Marked on figure 3 are the frequencies at which the Mu_{BC} lines would be expected for pure Si and pure Ge, calculated from the hyperfine parameters for Mu_{BC} given in [3]. The values in [3] are extrapolations to 0 K, however the Mu_{BC} hyperfine parameters for Si and Ge vary by less than 2% from their 0 K values for temperatures up to 150 K [35, 36], so the line positions would show little change at 70 K. The observed Mu_{BC} lines are broad, suggesting a spread of hyperfine parameters. This might be expected owing to the different bonding environments available to bond-centred hydrogen in alloy material; and indeed, modified environments for bond-centred hydrogen have been observed [23, 24] in low-Ge material. However, it can be seen qualitatively that the centres of each of the two Mu_{BC} lines shift away from their equivalent pure Si positions towards the pure Ge positions as the alloy becomes more Ge rich. This suggests that the Mu_{BC} hyperfine parameter in alloy material varies in a controlled way between the values seen in pure Si and Ge material.

More quantitatively, the Mu_{BC} precession signals were fitted in the time domain. The two lines were each fitted with a single frequency to represent the line's average position, and with a damping to represent the line width introduced by the spread in frequencies resulting from the distribution of hyperfine parameters. The isotropic component of the Mu_{BC} hyperfine parameter was then found from the line separation. Fits were made at several different temperatures for each alloy composition, with a final A_{iso} value for each alloy being found by averaging all values below 110 K (as discussed above, the Mu_{BC} A_{iso} value changes little in the 0–150 K region for Si and Ge). Figure 4 shows the Mu_{BC} A_{iso} versus alloy composition. It can be seen that this varies linearly with alloy composition over the entire alloy range, and a linear fit is shown in the plot.

3.2. Tetrahedral site (Mu_T) hyperfine parameter

Mu_T signals were clearly visible in high-transverse-field measurements in samples with $x = 0.11$ and 0.20, visible but much less clear in $x = 0.60$ and faintly visible in frequency spectra in $x = 0.45$ and 0.77 material. Longitudinal field repolarization measurements confirmed the presence of Mu_T in $x = 0.77$ material, with the weak transverse field signals indicating rapid relaxation of the species. RF-μSR was used to explore whether, in samples where Mu_T signals were weak in transverse field, muonium formation was delayed. Using

RF-μSR, Mu_T resonance lines could be seen in samples with $x = 0.09$ and 0.20, with no clear signals visible in $x = 0.45$ and 0.60 material—there was therefore no evidence of delayed formation in any of the samples studied. For some alloy samples, the Mu_T amplitude showed a strong temperature dependence. In particular, in the $x = 0.20$ material, no signals from either Mu_T or Mu_{BC} were visible below around 20 K in high transverse field, and in the $x = 0.11$ material there was a large dip in the observed amplitudes of both paramagnetic species around 10 K. A more detailed reporting and discussion of these features will be given elsewhere. Here we report only on the Mu_T hyperfine parameter deduced for alloy compositions and temperatures where Mu_T lines were visible in either transverse field or RF studies.

For the case of high-transverse-field measurements, the sum of the frequencies of the two Mu_T lines (ν_{12} and ν_{34}) gives the Mu_T hyperfine frequency directly [3]. Fits were therefore made in the time domain to the high transverse field spectra to extract frequency values for the Mu_T lines and obtain the temperature dependence of the Mu_T hyperfine parameter for $x = 0.11$ and 0.20. In the case of RF-μSR measurements, fits to resonance curves produced by sweeping the static field enabled the resonance position of the ν_{12} line to be determined, from which the Mu_T hyperfine parameter was found through calculation of the energy levels for a two-spin (electron and muon) system. RF-resonance signals tended to be stronger at lower temperatures, making the determination of hyperfine parameter values by this method easier below 150 K.

Figure 5(a) shows the Mu_T hyperfine parameter for alloy with $x = 0.20$, and figure 5(b) shows this for $x = 0.09$ and 0.11. For the $x = 0.20$ material, values from RF-μSR measurements agree well with those from high transverse field over the 20–150 K region where both types of measurements were made. Also shown in figure 5(a) are data for pure Si, taken from [37]. There are several points of interest. First, the values from the alloy material are lower than those from Si; in $x = 0.20$, the measured alloy value at 100 K is 1980 MHz, compared with 2010 MHz in Si, a reduction of 1.5%. However, the value in pure Ge is 2334 MHz, higher than Si, so that, if the Mu_T hyperfine parameter varied linearly with alloy composition between the elemental values, the expected value at composition $x = 0.20$ would be 2075 MHz. The measured alloy value is therefore almost 5% below that expected from linear extrapolation at 70 K. The same is true for the $x = 0.09$ and 0.11 alloys, which show values at 100 K of around 1982 MHz, also below the pure Si value. For all three alloys shown in figures 5(a) and (b), the difference from the pure Si value is greatest at the lowest temperatures measured, with the Mu_T hyperfine parameter seeming to come towards the value in pure Si as room temperature is approached.

It is therefore clear that the Mu_T hyperfine parameter is not a linear function of alloy composition at low temperatures as was found for the Mu_{BC} parameter. For $x = 0.6$, the weak Mu_T signal gives a hyperfine parameter of 1991(6) MHz at 50 K; Fourier spectra for $x = 0.45$ and 0.77 show faint Mu_T lines from which hyperfine parameter estimates of 1970(15) MHz at 75 K and 1999(25) MHz at 70 K respectively can be deduced (although the lines are too weak for time-domain fits in these two cases). Plotted in figure 4 is the Mu_T hyperfine parameter at 50 K (70 and 75 K for $x = 0.45$ and 0.77) versus alloy composition. The linear Mu_{BC} behaviour is contrasted with the very non-linear alloy composition dependence of the Mu_T parameter, which appears to drop well below that expected for a linear dependence for low Ge content, remaining low over much of the composition range, but which must then rise rapidly at large x values to the value expected for pure Ge.

The temperature dependence of the Mu_T hyperfine parameter is also of interest. It can be seen from figure 5 that, for pure Si [37], the parameter increases with decreasing temperature, reaches a maximum at around 100 K and then reduces slightly. In Ge, there is no such maximum, the hyperfine parameter just flattening off below around 30 K [37]. For the alloys

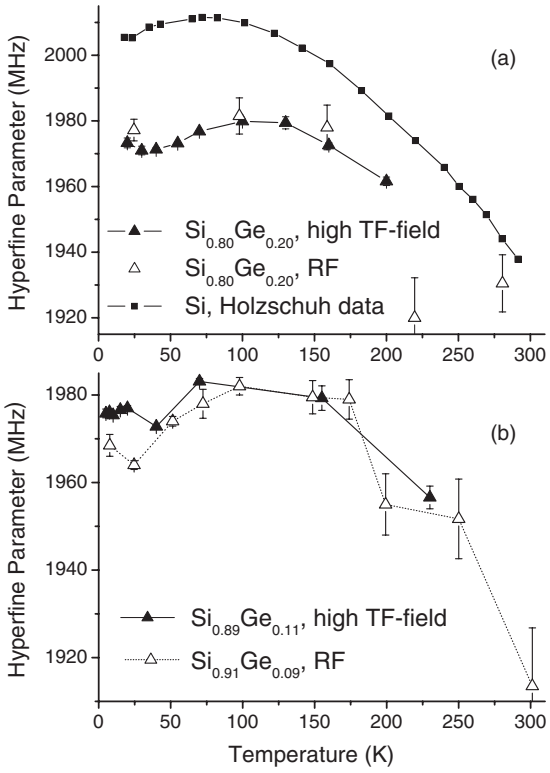

Figure 5. (a) Temperature dependence of the Mu_T hyperfine parameter from $x = 0.20$ alloy, measured using the high transverse field technique and RF-μSR. Also shown is the Mu_T hyperfine parameter from pure Si, taken from [37]. (b) Temperature dependence of the Mu_T hyperfine parameter for $x = 0.09$ and 0.11. The lines shown join the data points as guides to the eye.

shown here, a more complex low-temperature behaviour than that reported in [37] for Si is observed. As in Si, there is an increase in hyperfine parameter with decreasing temperature with a maximum at between 100 and 120 K followed by a reduction at temperatures below this. However, all three alloys also show signs of a further increase in hyperfine parameter at the lowest temperatures measured; there appears to be a minimum at between 25 and 40 K. (We note here that unpublished data [38] on the Mu_T hyperfine parameter in pure Si do reveal an upturn in the parameter value at around 15 K, which is not shown in the data of [37] and which can be compared with the similar features reported here and shown in figure 5 for $Si_{1-x}Ge_x$ alloy material).

4. Discussion

4.1. Variation of the Mu_{BC} and Mu_T hyperfine parameters with alloy composition

Figure 4 shows the observed linear variation of the isotropic component of the Mu_{BC} hyperfine parameter with alloy composition. It is of interest to note that, within bulk $Si_{1-x}Ge_x$ alloys across the composition range there is a random site occupancy of Ge and Si atoms, with no preferential ordering [14]. Also, the Ge–Ge, Ge–Si and Si–Si bond lengths are distinctly different and each varies linearly with alloy composition [14]. Implanted muons adopting

an immobile, bond-centred position therefore experience a random selection of bonding environments which overall show a linear variation with alloy composition but which, for a given alloy, depend upon the neighbouring atom species. This can account for both the width of the Mu_{BC} lines for a given alloy, and also the linear variation of hyperfine parameter across the alloy composition range.

Figure 4 also shows the very non-linear behaviour of the Mu_T hyperfine parameter with alloy composition. A qualitative, but plausible, explanation of this can be constructed based on expected differences in the rapid motion of the Mu atom among T sites in the pure materials. This motion is too rapid to have been properly characterized in either Si or Ge, but qualitative arguments backed by quantum chemical modeling imply that the T-site to T-site hop rate is much faster in Ge than in Si. The expected path for motion of a Mu atom between adjacent T-sites is through the centre of the puckered six-member ring separating adjacent tetrahedral cages. This opening is physically larger in Ge than in Si, since the distances from the centre of the ring to the six nearest host atoms are 2.32 and 2.24 Å, respectively. Further, the electronic charge distribution and the overall energy landscape within which a Mu atom moves are considerably flatter for Ge compared with Si [39, 40]. Both factors allow for faster Mu_T motion in Ge than in Si.

For a mobile species such as Mu_T, the measured hyperfine constant will be a dynamic average of the values for different local cage compositions weighted by the time spent in each local environment, rather than a static average based on probabilities of occurrence. Even a single Ge atom in any one of the four hexagonal rings controlling routes to neighbouring tetrahedral cages results in an enhanced hop rate in that particular direction. Thus, Mu_T traps more readily at T sites with all Si nearest neighbours than at T sites with one or more Ge neighbours. Therefore, the dynamic average heavily favours the all-Si local composition, thereby leading to a measured hyperfine Mu_T constant close to that of Si quite far into the alloy composition range. Exactly how such a dynamic average should vary with composition would require more detailed modeling of the barriers for Mu_T motion than has been attempted to date.

Although the modified phonon spectrum in an alloy certainly plays some role, a simple model to explain why the hyperfine constant is lowered in the alloy from the pure Si value can be formed by considering a static Mu_T and effects from small distortions to an all-Si cage introduced by a nearby Ge atom. Even though the Mu_T electronic wavefunction is no longer purely 1s, it retains full spherical symmetry and s-type character at an undistorted T-site. The lowest order effect of any small distortion lowering the tetrahedral symmetry of the cage, independent of precise details, is to introduce a small 2p component into this wavefunction. Since the overlap with nearest neighbours is (very weak but) covalent, this must lower the Fermi contact interaction at the muon, thus in turn lowering the isotropic part of the hyperfine interaction. Any small p-type character introduced into the hyperfine constants from such distortions is certainly averaged out, especially for a mobile Mu_T centre, leaving the measured interaction isotropic but lowered and broadened in the low-Ge-content alloy compared to pure silicon.

These two qualitative arguments provide a plausible explanation for the observed dependence of Mu_T hyperfine constants on composition in SiGe alloys, and suggest an appropriate starting point for detailed modelling of these effects.

4.2. Variation of the Mu_T hyperfine parameter with temperature

It is of interest to consider the observed temperature dependence of the Mu_T hyperfine parameter in $Si_{1-x}Ge_x$ alloys reported here in the light of previous models used to describe

observations in pure Si and Ge. The temperature dependence of both Mu_T and Mu_{BC} hyperfine parameters in Si and Ge for temperatures above around 70 K have been described previously in the literature by assuming that these species couple to the long-wavelength part of the Debye spectrum of acoustic phonons [35–37]. This simple model leads to hyperfine parameters which increase with decreasing temperature and which saturate to a temperature-independent value below around 40 K. The Ge hyperfine parameter of Mu_T, and the Mu_{BC} hyperfine parameter in both Si and Ge, are well described by this model down to around 5 K. In Si, as can be seen from figure 5(a), there is a maximum in the Mu_T hyperfine parameter at around 70 K followed by a decrease. Holzschuh [37] described this behaviour using the Debye model by assuming two different Mu_T sites with slightly different hyperfine frequencies, populated according to a Boltzmann distribution. A fit to the Mu_T parameter temperature dependence then yielded values for the shift in hyperfine frequency and energy difference between the two sites. Holzschuh justifies the possibility of two different Mu_T environments by noting that the coupling constant for the Mu interaction with the lattice within the model $C \propto m^{-\frac{3}{2}}$, where m is the atomic mass. A Mu_T site with a neighbouring ^{30}Si atom (possible for around 30% of Mu_T sites) would see a change in hyperfine parameter as compared with a Mu_T site surrounded totally by the isotopically abundant ^{28}Si atoms. Holzschuh calculates that a crystal of ^{30}Si would produce a Mu_T hyperfine parameter some 20 MHz lower than in ^{28}Si, all other things being equal.

For the $Si_{1-x}Ge_x$ alloy data reported here, whilst the Mu_T behaviour can possibly be explained for temperatures above around 30 K within the Holzschuh model, the low-temperature up-turn in hyperfine parameter observed in $x = 0.09$, 0.11 and 0.20 material cannot be described. This points to the Holzschuh model needing revision in order to explain the $Si_{1-x}Ge_x$ alloy data. We note also that the unpublished report [38] of the Mu_T hyperfine parameter in Si showing an upturn at low temperatures also suggests that the Holzschuh model needs further consideration. Whilst the Holzschuh model appears to fit the data for Si well for temperatures above around 25 K, its use of two different Mu_T sites with different hyperfine parameters is not intuitive, since it is believed that Mu_T is highly mobile at these temperatures. The use of the Debye model upon which the Holzschuh model is based is also questionable at low temperatures, where different phonon modes are being excited. Finally, even within the two-site model used by Holzschuh, it is not clear that the effect of heavier surrounding atoms has been correctly calculated. The Mu_T hyperfine parameter in a rigid lattice (heavier atoms) should be higher than that for a non-rigid lattice, whereas Holzschuh suggests a decrease in hyperfine parameter with heavier atoms.

A phonon-based model for the Mu_T hyperfine parameter temperature dependence in silicon and $Si_{1-x}Ge_x$ alloy material would seem to be correct, but additional treatment is needed beyond the Holzschuh model to account for the observed low-temperature behaviour. A revised model should allow for a more accurate description of the phonon modes including, for example, the preferential excitation of transverse acoustic modes at low temperatures, which leads to the negative thermal expansion of Si. That the Mu_T hyperfine behaviour in Si and $Si_{1-x}Ge_x$ might be modelled using a more complete phonon description, rather than the simple introduction of two Mu_T sites below 70 K as in the Holzschuh model, is suggested by the fact that the temperature dependence of the linear thermal expansion coefficient of silicon follows a very similar form to that of the Mu_T hyperfine parameter even at low temperatures. This can be seen in figure 6, where $[A_{Mu_T}\ (17\ K) - A_{Mu_T}(T)]$ is shown on the same graph as the thermal expansion coefficient (values from [41]). It can be seen that their forms are very similar, including both showing a turning point at around 70 K, indicating that it may be unnecessary to introduce two Mu_T sites to explain the drop in Mu_T hyperfine parameter in Si and $Si_{1-x}Ge_x$ as the temperature is lowered below 70 K. In fact, the Si linear thermal

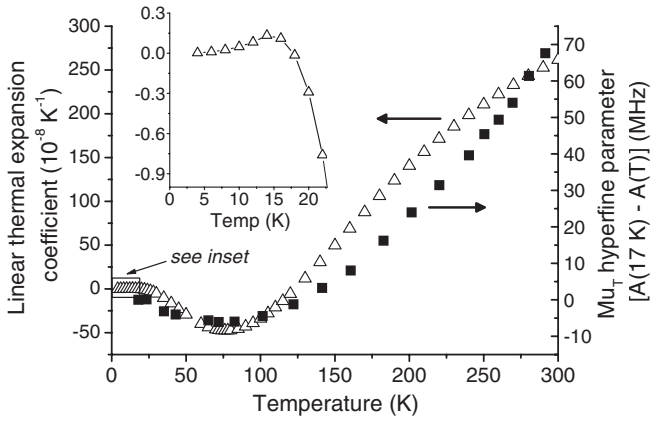

Figure 6. Comparison of the temperature dependence of the Mu_T hyperfine parameter in Si (taken from [37], right-hand axis) with the silicon linear thermal expansion coefficient (taken from [41], left-hand axis). The inset shows the linear thermal expansion coefficient below 22 K.

expansion coefficient undergoes a second turning point at around 15 K (see inset to figure 6), albeit of small amplitude, so it is not surprising that recent, more careful measurements of the Si hyperfine parameter also appear to show a turning point at this temperature [38].

We therefore conclude that the Holzschuh model for the low-temperature behaviour of the Mu_T hyperfine parameter in Si, based on different Mu_T sites, is most likely not complete, and that a full modeling of Si phonons and their interaction with Mu_T could provide a more accurate description. Such a description is also necessary to account for muonium behaviour in $Si_{1-x}Ge_x$ alloy material reported here. It is probable that, particularly at temperatures below 20 K or so, account must also be taken of the diffusion rate and lattice site of Mu_T in addition to phonon effects, as these are likely to influence the hyperfine parameter to an increasing extent as the temperature falls. Further work is needed to establish an appropriate model which accounts fully for the effects of phonons and the Mu_T motion.

5. Summary

We have measured the Mu_T and Mu_{BC} hyperfine parameters in bulk $Si_{1-x}Ge_x$ alloy material as a function of alloy composition and temperature. The average value of the Mu_{BC} parameter shows a linear variation with alloy composition, which can be understood considering the linear variation of bond lengths across the alloy composition range. The Mu_T parameter variation is non-linear with alloy composition, and a qualitative explanation for this has been given based on the difference in mobility of Mu_T in Si and Ge together with the effects on the Mu_T wavefunction of lattice distortions in alloy material. The temperature dependence of the Mu_T hyperfine parameter in $Si_{1-x}Ge_x$ alloys is more complex than has been previously suggested for pure Si, and suggests it is governed by interaction with phonon modes in a more involved way than has been described by previous models. A more complete model is needed to provide an accurate description.

Acknowledgments

PJCK would like to thank the EPSRC (grant GR/N64977/01) for support for this work, and SPC would like to thank the EPSRC (grant GR/R53067/01) for enabling development of the

RF-μSR technique. RLL would like to thank the US NSF (grant DMR-0102862) and the Robert A Welch Foundation (grant D-1321). We would like to thank Steve Cox and Stefan Estreicher for useful discussions.

References

[1] Van de Walle C G and Neugebauer J 2003 *Nature* **423** 626
[2] Davis E A and Cox S F J (ed) 1996 *Protons and Muons in Materials Science* (London: Taylor and Francis)
[3] Patterson B D 1988 *Rev. Mod. Phys.* **60** 69
[4] Hitti B, Kreitzmann S R, Estle T L, Bates E S, Dawdy M R, Head T L and Lichti R L 1999 *Phys. Rev.* B **59** 4918
[5] Lichti R L, Cox S F J, Chow K H, Davis E A, Estle T L, Hitti B, Mytilineou E and Schwab C 1999 *Phys. Rev.* B **60** 1734
[6] Cox S F J, Davis E A, Cottrell S P, King P J C, Lord J S, Gil J M, Alberto H V, Vilão R C, Piroto Duarte J, Ayres de Campos N, Weidinger A, Lichti R L and Irvine S J C 2001 *Phys. Rev. Lett.* **86** 2601
[7] Davis E A, Cox S F J, Lichti R L and Van de Walle C G 2003 *Appl. Phys. Lett.* **82** 592
[8] Hofmann D M, Hofstaetter A, Leiter F, Zhou H, Henecker F, Meyer B K, Orlinskii S B, Schmidt J and Baranov P G 2002 *Phys. Rev. Lett.* **88** 045504
[9] Brunner K 2002 *Rep. Prog. Phys.* **65** 27 and references therein
[10] Yonenaga I 2005 *J. Cryst. Growth* **275** 91
[11] Yonenaga I 1999 *Physica* B **273/274** 612
[12] Yonenaga I, Akashi T and Goto T 2001 *J. Phys. Chem. Solids* **62** 1313
[13] Franz M, Pressel K, Barz A, Dold P and Benz D W 1998 *J. Vac. Sci. Technol.* B **16** 1717
[14] Yonenaga I, Sakurai M, Sluiter M H F and Kawazoe Y 2004 *Appl. Surf. Sci.* **224** 193
[15] Franz M, Pressel K and Gaworzewski P 1998 *J. Appl. Phys.* **84** 109
[16] Gaworzewski P, Tittlebach-Helmrich K, Penner U and Abrosimov N V 1998 *J. Appl. Phys.* **83** 5258
[17] Béraud A, Kulda J, Yonenaga I, Foret M, Salce B and Courtens E 2004 *Physica* B **350** 254
[18] Atabaev I G 2001 *Comput. Mater. Sci.* **21** 526
[19] Ruzin A, Marunko S and Gusakov Y 2004 *J. Appl. Phys.* **95** 5081
[20] Yonenaga I, Nonaka M and Fukata N 2001 *Physica* B **308–310** 539
[21] Markevich V P, Peaker A R, Coutinho J, Jones R, Torres V J B, Öberg S, Briddon P R, Murin L I, Dobaczewski L and Abrosimov N V 2004 *Phys. Rev.* B **29** 125218
[22] Hayama S, Davies G, Tan J, Markevich V P, Peaker A R, Evans-Freeman J, Vernon-Parry K D and Abrosimov N V 2003 *Physica* B **340–342** 823
[23] Bonde Nielsen K, Dobaczewski L, Peaker A R and Abrosimov N V 2003 *Phys. Rev.* B **68** 045204
[24] Pereira R N, Dobaczewski L and Bech Nielsen B 2003 *Physica* B **340–342** 803
[25] Hourahine B, Jones R, Öberg S, Briddon P R and Frauenheim T 2003 *J. Phys.: Condens. Matter* **15** S2803
[26] Maric Dj M, Meier P F and Estreicher S K 1993 *Phys. Rev.* B **47** 3620
[27] Doring K-P, Haas N, Haller E E, Herlach D, Jacobs W, Krauth M, Orth H, Rosenkranz J, Seeger A, Vetter J, Arnold K P, Aurenz T and Bossy H 1983 *Physica* B **116** 354
[28] King P J C and Yonenaga I 2001 *Physica* B **308–310** 546
[29] King P J C, Lichti R L and Yonenaga I 2003 *Physica* B **326** 171
[30] King P J C, Lichti R L and Yonenaga I 2003 *Physica* B **340–342** 835
[31] Blundell S J 1999 *Contemp. Phys.* **40** 175
[32] Lynch M C, Cottrell S P, King P J C and Eaton G H 2003 *Physica* B **326** 270
[33] Cottrell S P, Cox S F J, Scott C A and Lord J S 2000 *Physica* B **289** 693
[34] Johnson C, Cottrell S P, Ghandi K and Fleming D G 2005 *J. Phys. B: At. Mol. Opt. Phys.* **39** 119
[35] Blazey K W, Brown J A, Cooke D W, Dodds S A, Estle T L, Heffner R H, Leon M and Vanderwater D A 1981 *Phys. Rev.* B **23** 5316
[36] Blazey K W, Estle T L, Holzschuh E, Odermatt W and Patterson B D 1983 *Phys. Rev.* B **27** 15
[37] Holzschuh E 1983 *Phys. Rev.* B **27** 102
[38] Kreitzmann S R 2005 *TRIUMF Data* unpublished
[39] Estreicher S K and Maric Dj M 1993 *Phys. Rev. Lett.* **70** 3963
[40] Estreicher S K 1995 *Mater. Sci. Eng.* **R14** 319
[41] Lyon K G, Salinger G L and Swenson C A 1977 *J. Appl. Phys.* **48** 865